





A Small Actively Controlled High-resolution Spectrograph Based on Off-the-shelf Components

H. R. A. Jones¹ , W. E. Martin¹, G. Anglada-Escudé² , R. Errmann¹ , D. A. Campbell¹, C. Baker³, C. Boonsri⁴, and P. Choochalem¹

¹ Centre for Astrophysics Research, University of Hertfordshire, College Lane, Hatfield AL10 9AB, UK; h.r.a.jones@herts.ac.uk

² Institute of Space Sciences, Campus UAB, Carrer de Can Magrans, s/n E-08193 Barcelona, Spain

³ Queen Mary University of London, Mile End Road, London AL10 9AB, UK

⁴ National Astronomical Research Institute of Thailand, 260 Moo 4, T. Donkaew, A. Maerim, Chiang Mai, 50180, Thailand

Received 2020 July 24; accepted 2020 November 5; published 2021 January 26

Abstract

We present the design and testing of a prototype in-plane echelle spectrograph based on an actively controlled fiber-fed double-pass design. This system aims to be small and efficient with the minimum number of optical surfaces—currently a collimator/camera lens, cross-dispersing prism, grating and a reflector to send light to the detector. It is built from catalog optical components and has dimensions of approximately 20×30 cm. It works in the optical regime with a resolution of $>70,000$. The spectrograph is fed by a bifurcated fiber with one fiber to a telescope and the other used to provide simultaneous Thorium Argon light illumination for wavelength calibration. The positions of the arc lines on the detector are processed in real time and commercial auto-guiding software is used to treat the positions of the arc lines as guide stars. The guiding software sends any required adjustments to mechanical piezo-electric actuators which move the mirror sending light to the camera removing any drift in the position of the arc lines. The current configuration using an sCMOS detector provides a precision of 3.5 milli-pixels equivalent to 4 m s^{-1} in a standard laboratory environment.

Unified Astronomy Thesaurus concepts: [Astronomical instrumentation \(799\)](#); [Radial velocity \(1332\)](#); [Spectrometers \(1554\)](#)

1. Introduction

The achievement of meter-per-second radial velocity precision is one of the major technological breakthroughs of recent decades. Although this effort is sometimes viewed as driven by the search for extra-solar planets following the discovery of the first promising signals (e.g., Latham et al. 1989; Wolszczan & Frail 1992), the quest for highly accurate radial velocity measurements had been under development for many decades. The path from the suggestion that stellar velocities might be accurately calibrated (Struve 1952), to solar studies (Becker 1976; Koch & Woehl 1984) to pioneering stellar observations using Hydrogen Fluoride gas cells (Campbell & Walker 1979; Campbell et al. 1988) to sub- m s^{-1} with ESPRESSO (e.g., Pepe 2018), long-term several m s^{-1} rms (and short-term sub- m s^{-1} measurements with ESO 3.6 m/HARPS (e.g., Pepe et al. 2000), Keck/HIRES, e.g., Vogt et al. 1994; Butler et al. 1996), Magellan/PFS (e.g., Crane et al. 2006), HET/HRS (e.g., Tull 1998), TNG/HARPS-N (Cosentino et al. 2012) and VLT-UVES (e.g., Butler et al. 2019) and is one that leads through several generations of similar spectrographs, detectors, and calibration methodologies.

Although the instruments have not changed dramatically, the ongoing improvements in the production of accurate and precise radial velocities has arisen through the combination of a number of factors. That is, keeping instruments stable over long periods of time along with the ability to accurately calibrate spectra and to effectively reduce astronomical spectra. However, the large beam sizes of large telescopes has tended to mean that large bespoke optics are required for the optical elements, e.g., HIRES on Keck uses a mosaic of three gratings with a size of 1×4 foot (Vogt et al. 1994). The need for mosaic gratings and bespoke large optics continues to contribute to the ongoing high cost of such instruments, e.g., 23.7 MEuros⁵ for ESPRESSO and might further escalate as such instruments are built for larger telescopes.

We contribute to this series of work by investigating some alternative approaches for the configuration of a high-resolution spectrograph. We describe our experiments with a laboratory-based, test-bed, high-resolution spectrograph using traditional components. The goal of this paper is to demonstrate new design features which lead to a reduction in the size and cost without modest impact on performance. In the long term it can be envisaged the popularity of high resolution spectrographs will continue to build particularly if their cost/performance can be



Original content from this work may be used under the terms of the [Creative Commons Attribution 3.0 licence](https://creativecommons.org/licenses/by/3.0/). Any further distribution of this work must maintain attribution to the author(s) and the title of the work, journal citation and DOI.

⁵ http://obswww.unige.ch/~pepe/Repository/DRD03_Executive%20Summary_VLT-TRE-ESP-13520-0037_Iss3.pdf

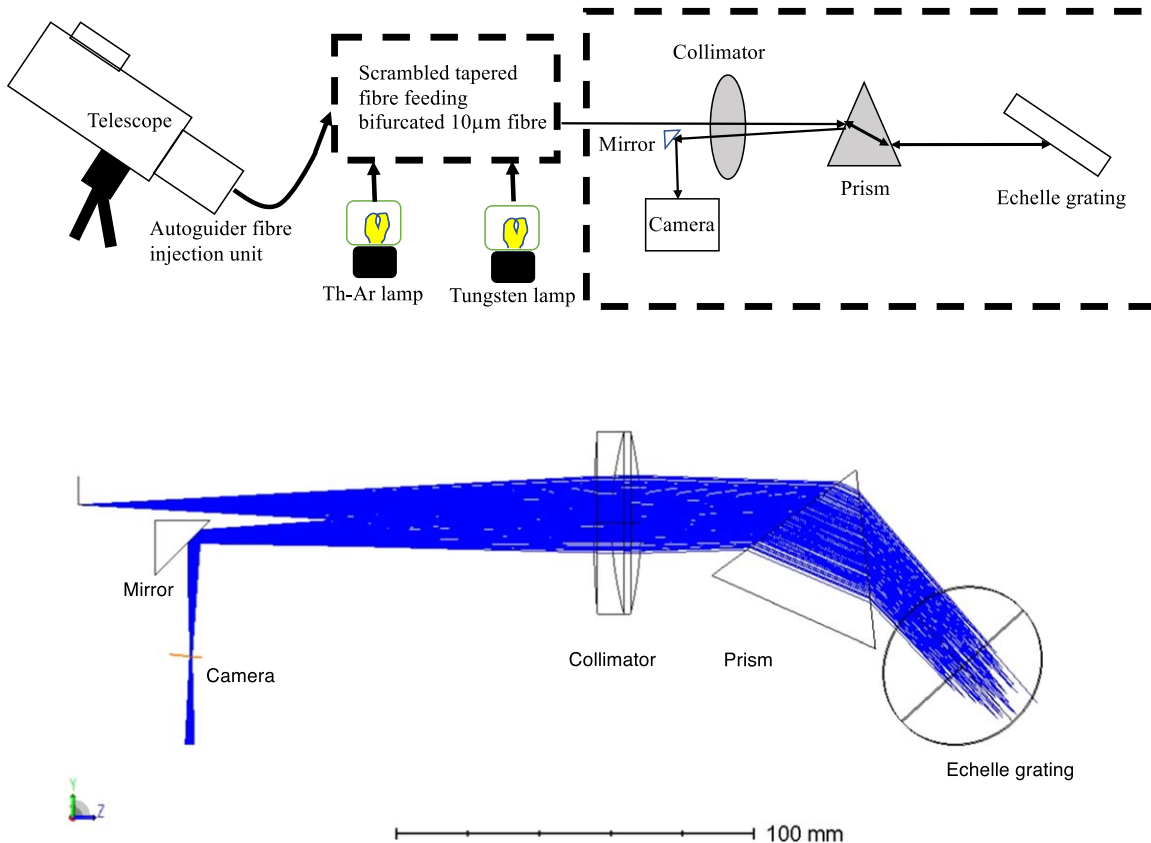


Figure 1. Top—schematic of the components of the instrument. A variety of different options are available within the fiber feed arrangements to the spectrograph. Once the fiber enters the spectrograph the light path is fixed with double passes of the collimator and the prism. The angular changes within collimator and dispersing prism are exaggerated for illustration. Bottom—optical layout from a Zemax model is illustrated. The figure is a top view in the plane of the echelle cross-dispersion plane. The black outlines are schematics of the optical components.

improved so that they can be deployed much more widely and following the concept of Lovis et al. (2017) offer one route to exploit the potential for high resolution integral field spectroscopy behind a high resolution adaptive optics instrument.

Some of our new design features are to be deployed and built into the as EXOhSPEC (EXOplanet High resolution SPECTrograph) instrument for the 2.4 m Thai National Telescope. The spectrograph is envisaged as fiber-fed with a resolution of greater than 70,000 and designed to be a workhorse high resolution spectrograph. The optical design and Zemax tolerancing analysis of this spectrograph is described in Lhospice et al. (2019) and the finite element analysis for the collimator design in Kawinkij et al. (2019). Our currently preferred methodology for achieving efficient focal reduction is through efficient tapering of the input fiber from the telescope as presented by Choochalem et al. (2021). Alongside these efforts we have developed a data reduction pipeline (Erman et al. 2020) which can be used for EXOhSPEC but is specifically built with the flexibility to examine data from our laboratory prototypes. In Section 2, we outline and present the basic spectrograph, considering its design and components. In

Section 3, we describe our initial set of components and first test results considering modal noise, temperature, throughput and active stabilization.

2. Outline Design

The construction of a high resolution spectrograph aimed at measuring precision radial velocities on a very limited budget, required that our pathfinder spectrographs work in the optical regime where detectors, optical equipment and their coatings are much more affordable. The spectrograph uses standard optical mounting hardware on an 4×2 foot optical bench. It is located in the Applied Optics Laboratory on the College Lane campus of the University of Hertfordshire. In Figure 1 we illustrate a schematic layout and the outline Zemax design of the spectrograph. In Figure 2 we illustrate one of our initial implementations of the spectrograph along with the various components of the spectrograph.

2.1. Telescope and Laboratory

We have arranged the laboratory to be fed by fiber optic cable from a relatively sheltered nearby first floor flat roof of an adjacent

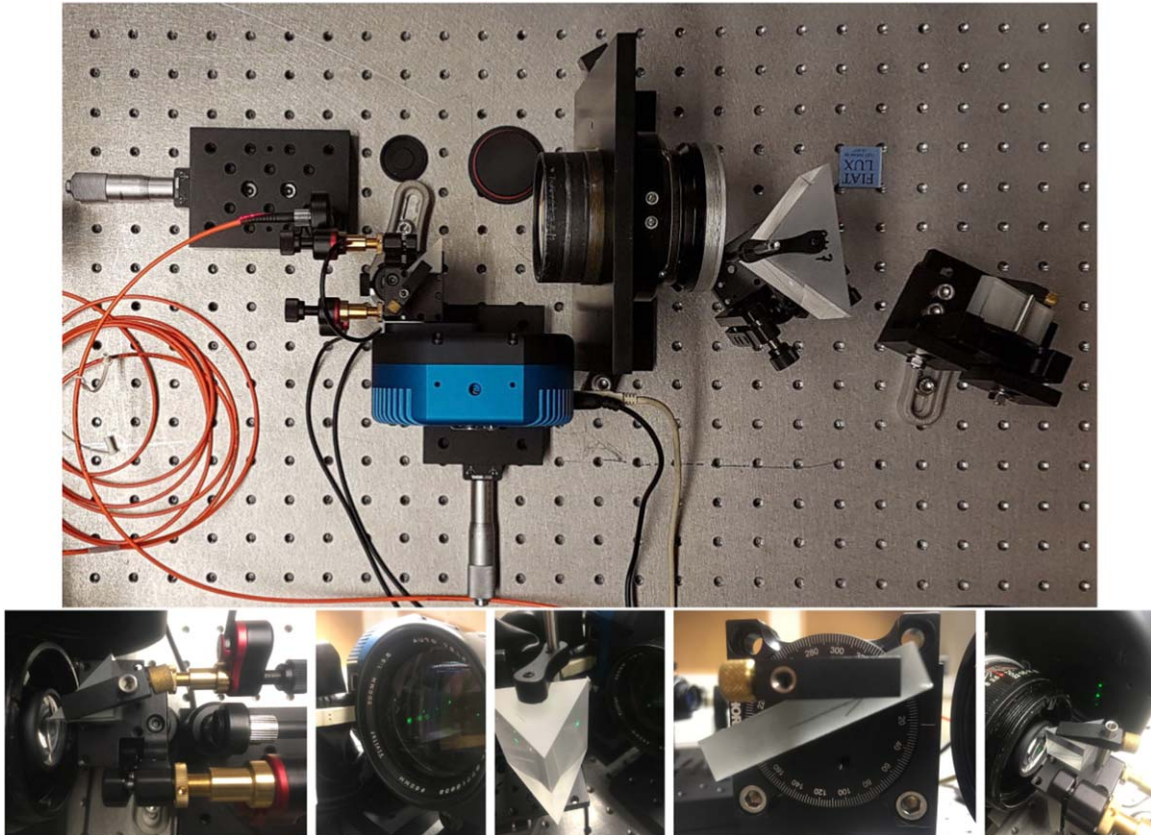


Figure 2. The image shows the layout of instrument on the bench. Following the light path: the fiber input (orange) is toward the top-left, it passes through the camera lens top-middle, the cross dispersing prism top-right, grating middle-left. The light then returns by almost the same path and is reflected by the pickoff prism mirror immediately before the camera in the bottom-left. The lower images show the individual optical components from left to right: fiber input (on the right-hand side with red, gold and black piezo actuators above and below and also showing camera lens on left-hand side), camera lens—Vivitar, 200 mm f3.5 telephoto lens, cross-dispersing prism (and camera lens), grating, pickoff mirror (a silvered prism, with camera lens to the left and detector to the right illuminated with laser diode diffraction spots).

building. There we added a Celestron 8 inch telescope, with a SkyWatcher EQ3-2 Pro Synscan mount. Although it is in a highly light-polluted area of campus, overlooked on all sides by office windows, suffers from vibrations caused by a nearby heat exchanger and with a rather restricted view of the sky it can in principle provide access to the Sun, Moon and potentially bright stars. We attach a core graded-index $50\ \mu\text{m}$ FC/PC connectorised fiber to the telescope using a Shelyak fiber injection unit (PF0018 F/6 $50\ \mu\text{m}$ injection unit and M42 T adapter to the telescope).

The laboratory temperature control is tied to a central building control system and the ambient temperature of the room is constrained to within approximately $2\ ^\circ\text{C}$ on a variety of timescales so we monitor temperature and humidity changes at the apparatus. In particular, the issue of hard to control atmospheric changes has encouraged us to investigate active control as a solution for the spectrograph stability. This can be thought of as an alternative solution to the usual deployment of precise high resolution spectrographs into a vacuum tank,

2.2. Active Stabilization

Feedback loops are widely deployed in astronomy. These are widely found in telescope guiding systems where a variety of closed loop servo-actuated systems are used to optimize the response of a telescope to the wind and other environment noise. This allows them to maintain precise pointing position on the sky. Such techniques are also sometimes used in optical astronomy. For example, the “ultra-stable” cryostat used by the ESPRESSO instrument, e.g., Lizon et al. (2016) provides continuous optical centroiding corrections based on temperature and pressure sensors inside the detector dewar. This enables the detection and correction of instability and drift of image motion. This detector system provides $2\ \text{nm}$ rms centroid stability and is a key part of the long-term $50\ \text{cm s}^{-1}$ precision achieved by ESPRESSO (e.g., Pepe et al. 2020). Ultimately, it might be to deploy some of the techniques developed by the atom interferometer experiments (e.g., Peters et al. 2001) which have led to a measured noise of better than $10^{-19}\ \text{m}$ in differential arm length over a wide range of frequencies

(30–3000 Hz) by the gravitational wave experiments (e.g., Buikema et al. 2020) providing a particularly stark example of the power of the application of closed loop technology (e.g., Bond et al. 2016).

Conventional designs of high-precision echelle spectrographs rely principally on good passive athermal designs and stable mechanical components. Environmental variables such as temperature, pressure and vibration are isolated from the spectrograph by insulation, inert gas filling or vacuum operation and vibration damping arising from massive and/or highly damped materials. The addition of active control of a few parameters such as distances between components or deflection angles of certain components can relieve the need for expensive and/or massive components to achieve the same level of overall stability. An active metrology scheme whereby, for example, the distance between two components is measured with (commercially available) laser interferometers and used to drive a piezoelectric motion transducer to stabilize the optical distance can offer compensation for both temperature and pressure effects in the spectrometer. With careful passive design and optimum optical configurations, this approach might offer considerable benefit and potentially offer a retrofit solution to improve the performance of existing spectrometers.

A complementary approach to athermal design and stable mechanical components is to wonder how to produce a stable spectrum position on the sensor? If a reference spectral source is imaged through the spectrometer then the position of this (these) source(s) in the dispersed image on the detector can be used to produce an error signal to drive a component of the spectrometer so that the image remains fixed in position on the detector. If the object spectrum is imaged through the same optical path then it too is stabilized. Note that to zeroth order it does not matter what is between the spectrometer input and output. Obviously it will be good design practice to have a stable optical/mechanical design in order to reduce the range of the control corrections needed. To first order, the spectrum on the detector is stabilized to the limiting stability of the reference source. The remaining issues for stability will be second and third order effects due to two principal factors: (a) the angle/position of the optical path through the spectrometer will be changing with the corrections and (b) changes in the dispersion of the spectrometer. There will be slight differences in the design approach to minimize aberrations from third order effects such as the change of dispersion of the lens and prism with temperature and of the surrounding gas environment. Changes in the dispersion of the spectrometer may be approached in a similar way that achromatic lenses are designed, i.e., introduction of components which cancel the overall dispersion variations with temperature or pressure. The two primary requirements for this design are a usable stable reference source and a control loop with sufficient capability to affect the necessary corrections. So for example, ThAr lamp lines which are routinely used as the reference sources for precision spectrographs can be used as the reference

source for such active correction and this is a methodology we explore.

2.3. Preliminary Optical Design

One of the key issues for high precision spectrographs is that they must be stable on all timescales which might be of interest for astronomical phenomena. When considering exoplanets this might be from hours to hundreds of years (e.g., Feng et al. 2019). Both simultaneously calibrated spectrographs such as HARPS and Iodine stabilized spectrographs such as HIRES work on the premise that the optical arrangement should be as stable as possible. So in the case of common user spectrographs like HIRES, a bespoke calibration procedure is required to ensure that each night begins and ends with ThAr lines falling on exactly the same position on the detector. HARPS achieves this with extreme temperature and pressure control along with complete isolation of the spectrograph from any human interaction.

There are many different successful designs available for us to develop from. We seek to benefit from these and in particular we take inspiration from the HARPS (Pepe et al. 2000) and PFS (Crane et al. 2006) instruments due to their exquisite performance over more than a decade of operation. Both of these designs are themselves derived from several similar previous instruments with the fundamental designs and grating and echelle relationships being laid out in the literature, e.g., Schroeder (1967, 1970), Schroeder & Anderson (1971). Given that we have a laboratory available some distance from any telescope, a fiber feed like HARPS was desirable. On the other hand, the small size and re-use of optical components provided by a double-pass design was particularly appealing from the PFS design.

One of the major cost items of a high resolution spectrograph is usually its echelle grating. In the case of HARPS, its grating is constructed from two gratings mosaiced together to give a total area of 84×21.4 cm. In order to scale down the required grating size we can make use of the well established literature results that the resolution of a spectrograph is proportional to the angle of the slit opening (fiber diameter) as seen from the collimator (e.g., Schroeder 1987). Given that we are focused on a high resolution instrument, we choose a resolution of 10^5 close to that of HARPS in Table 1 to show a HARPS-like configuration as well as the case for a catalog Thorlabs grating (GE-2550-0363) to emphasize that by making the fiber diameter smaller for a fixed numerical aperture and blaze angle we can use a smaller echelle grating.⁶

Thus taking the HARPS spectrograph as a model we might hope to emulate its resolution and approximate optical characteristics based on line 2 or 4 of the table by ensuring

⁶ Presented in more detail at http://star.herts.ac.uk/exohspec/design_outline.pdf.

Table 1
Beam Diameter, Grating Length and Ruled Area Requirements for Different Fiber and Grating Parameters

Resolution ($\lambda/\delta\lambda$)	Fiber Diameter (μm)	Numerical Aperture (—)	Blaze Angle (deg)	Beam Diameter (cm)	Grating Length (cm)	Ruled Area (cm^2)
<i>10^5</i>	<i>50</i>	<i>0.22</i>	<i>75</i>	<i>19.7</i>	<i>76.0</i>	<i>1498</i>
10^5	10	0.22	75	4.0	15.2	60.8
10^5	50	0.22	63	37.5	82.4	3088
10^5	10	0.22	63	7.6	16.5	125

Note. The first line of the table is given in italic and approximately reproduces the effective size of the HARPS beam based on its 84×21.4 cm grating used at a blaze angle of 75 deg mosaic. A blaze angles of 63 degrees is also chosen as a representative case, e.g., Thorlabs GE-2550-0363.

Table 2

The Approximate Performance of Main Spectrograph Components Noting that Most have Very Considerable Wavelength Dependence and Performance Trade-offs

Component	Manufacturer Catalog Number	Transmission (%)
Fiber feed	FG010LDAFBUNDLE	75
Scrambling	Tektronix AFG1022	50
Echelle Grating	Newport 53019ZD01-413E (27 grooves/mm, 70 deg blaze)	40
Collimator	Thorlabs AC254-050-B and AC254-200-B	90
Cross Dispersing Prism	80 mm N-BK7 60 deg (modified Thorlabs PS854)	50
Turning mirror	Thorlabs MRA20-G01	95
Camera	Photometrics Prime BSI sCMOS (2048 \times 2048, 6.5 μm pixels)	70
Overall	460–880 nm, Resolution 82500, Sampling 4–13 pix per FWHM	4

Note. The acquisition and guidance of light from the telescope is omitted from this table.

that the numerical aperture of the beam is preserved say when moving from a 3.6 m telescope to a 0.7 m telescope by rescaling the size of the input beam accordingly by a factor of five (3.6/0.7). Geometrical optics suggests that this would lead to a loss of light proportional to the change in area of the beam size (e.g., Haynes et al. 2012) resulting in most of the light being lost. However, based on the work of Choochalerm et al. (2021) we might use suitably tapered graded index fibers to reduce this beam size by a factor of 5 with perhaps less than a factor of two efficiency loss.

3. Spectrograph Components

We now discuss our consideration for different spectrograph components used for our tests along with their approximate transmissions in Table 2. A schematic of the apparatus is given in Figure 1.

3.1. Echelle Grating

Following Section 2.2, with the reduction of size of the required grating by a factor of five fits approximately with available off-the-shelf gratings like the Newport 53019ZD01-413E (27 grooves/mm, 70 deg blaze) with dimensions: 6×15 cm for a few thousand dollars or with reduced resolution using the volume produced Thorlabs GE-2550-0363 with 31.6 grooves/mm, 63 deg blaze, 2.5×5.0 cm for a few hundred dollars. The echelle is mounted facing downwards in order to minimize exposure to dust.

This brings a consequent reduction in the size of the lens and cross-disperser optics to the scale of standard catalog components and in particular the utility of standard telescope lenses. While this has the potential to yield very significant cost savings and clarity of performance due to using well-characterized mass produced components, there are a number of issues that might arise from doing this. For example, the camera optics have to be of high quality in order to keep the aberrations smaller than the fiber image size. In order to investigate these and other potential other issues we have built several prototypes.

3.2. Collimator—Camera Lens and Cross Dispersing Prism

The spectrograph optics are used in double-pass and so act both as collimator and camera lens. The required optics are all spherical. Our setup has thus far been with off-the-shelf camera lenses (such as the 200 mm Vitkar lens shown in Figure 2) or the achromatic doublet collimator and focusing lenses (from Thor Labs with 650–1050 nm coatings, AC254-050-B and AC254-200-B).

In our double-pass configuration, the quality and performance of this lens is rather critical. The camera optics do have to be of high enough quality in order to keep the aberrations smaller than the fiber image size. Any significant misalignment or chromaticity is easily seen in the output spectra where the line shape of calibration lines can be compared between the center and the edges. Our current camera layout does suffer from some coma and this variation of the spot shape over the camera field imposes a limits on the resolution and achievable

radial velocity precision in our system. We have performed Zemax calculations and find that the coma we find is in line with the expectation for doublet lenses. Details of similar calculations for an improved triplet design are presented in detail in Lhospice et al. (2019) and Kawinkij et al. (2019). We also have a separate project to deliver a prototype based on a highly corrected small double Gauss lens which is laid out elsewhere, e.g., Baker et al. (2019). While the camera lens does limit the utility of our current setup, the current achromatic doublet implementation was judged sufficient for our initial tests.

We use an equilateral dispersive prism in order to cross disperse the beam. We have used a few different dispersing prisms particularly the Thorlabs PS854 (F2 50 mm). We now use a modified version of this, a N-BK7 anti-reflection coated 60 deg prism (F2 80 mm). In principle a VPH grating (e.g., Seifahrt et al. 2018) would offer improved throughput but in the development stage prisms are readily available, easy to handle and offer a variety of dispersions, sizes and coatings.

3.3. Detector

A key driver in spectrograph design is the detector. The HARPS detector⁷ choice of two EEV type 44-82 CCDs with 15 μm pixels leads to a pixel oversampling of around 4. These relatively large pixels and apparently excessive oversampling are a key element in the success of HARPS in the sense that it can utilize CCDs where every pixel produces high dynamical range and that the point-spread function is always fully sampled and far less prone to detector inhomogeneities and irregularities (e.g., Butler et al. 2019). In order to match these characteristics we need a large format camera with around 3 μm pixels. Such a small size is rather smaller than supplied for conventional CCD detectors. In comparison with the HARPS CCDs, the newer E2V 290-99 in use for ESPRESSO, PEPSI, EXPRES and MAROON-X has approximately fivefold increase in pixels for an individual device, a reduction from 15 to 10 μm pixels for similar well-depth gain read-out noise configurations, improved quantum efficiency by around 10% (over the relevant wavelength range) with apparently similar linearity, charge transfer efficiency and cosmetic properties (Calderone et al. 2016). While these devices have excellent performance characteristics, the range of applications that they are used for is relatively limited and so professional astronomical grade CCDs sold by companies such as Teledyne (E2V) have a unit costs in excess of 100k dollars each. In recent years an alternative image recording technology CMOS has become widely available with a relatively low cost per pixel in comparison to CCDs. While scientific grade CMOS devices (sCMOS) have rapidly improved they have drawbacks for astronomical purposes. sCMOS can have high read noise

and dark current, they generally have a rather small dynamic range and perhaps significant intrapixel non-uniformities (Zhan et al. 2017). However, some of these sCMOS devices are deemed as mature enough to be used for future space missions such as JUICE (e.g., ESA 2014).

For our experiments we have used (1) a QSI 532ws-M1 camera with 2184×1472 6.8 μm pixels and (2) a reburbished Photometrics Prime BSI sCMOS with 2048×2048 6.5 μm pixels. These have been set to typically give 70 orders with a wavelength coverage from 460 to 880 nm. Different order spacings and numbers of orders are readily achieved by using different cross-dispersing prisms. The specifications of the CCD are somewhat better in most respects than the sCMOS but the negligible read time of the sCMOS makes it very convenient in a laboratory setting. However, the use of two amplifiers (for each pixel) to produce the 16 bit output of the sCMOS gives rise to significant nonlinearity, plotted in Figure 3. Photometrics (2020, private communication) have investigated different versions of their firmware which can improve the nonlinearity to 2%. Although this level of linearity is comparable to the CCD, the CCD nonlinearity is smooth whereas the sCMOS has a more complex correction of the functional form of the nonlinearity between the amplifiers. A correction routine in the data processing code is used to linearize the signal. The cameras are both air or water cooled and are typically run at -30°C from Cyanogen Imaging® MaxIm DL Pro⁸ version 6.18. Both cameras take in excess of an hour for their temperatures to stabilize.

3.4. Spectrograph Setup and Alignment

In order to align our spectrograph, we follow the following sequence of steps: (1) Use a green laser diode (e.g., Thorlabs CPS532 Laser diode module, 532 nm) to set up a straight path (constant height, aligned with the optical bench). (2) Insert the prism, rotate it and align so that the reflected/transmitted light does not change height. (3) Insert the lens, adjust the height, position, and angles so that all surface reflections of the lens hit the laser. (4) Find the minimum deviation angle of the prism: rotate and observe the minimum spot deviation. (5) Insert the grating so that the spot hits approximately the center of the grating and rotate it so that the reflected orders are approximately in the plane of the laser. (6) Insert the fiber holder, so that the laser passes through the center. (7) Attach the fiber illuminated with a red laser diode (e.g., Thorlabs CPS635S Laser diode module, 635 nm) and find the focal spot (the spectrum of the laser diode is in focus at the fiber end). (8) Move the fiber 2 mm out of the center. (9) Center the grating and check that the reflection hits the reflection grating. (10) Center the spectrum on the camera. (11) Put white light through the system to focus the camera. A rotation of the camera might be necessary. (12) The final focusing is done

⁷ <http://www.eso.org/sci/php/optdet/instruments/harps/FDR-Harps-detectors.pdf>

⁸ Cyanogen Imaging® MaxIm DL Pro is a registered trademark of Diffraction Limited.

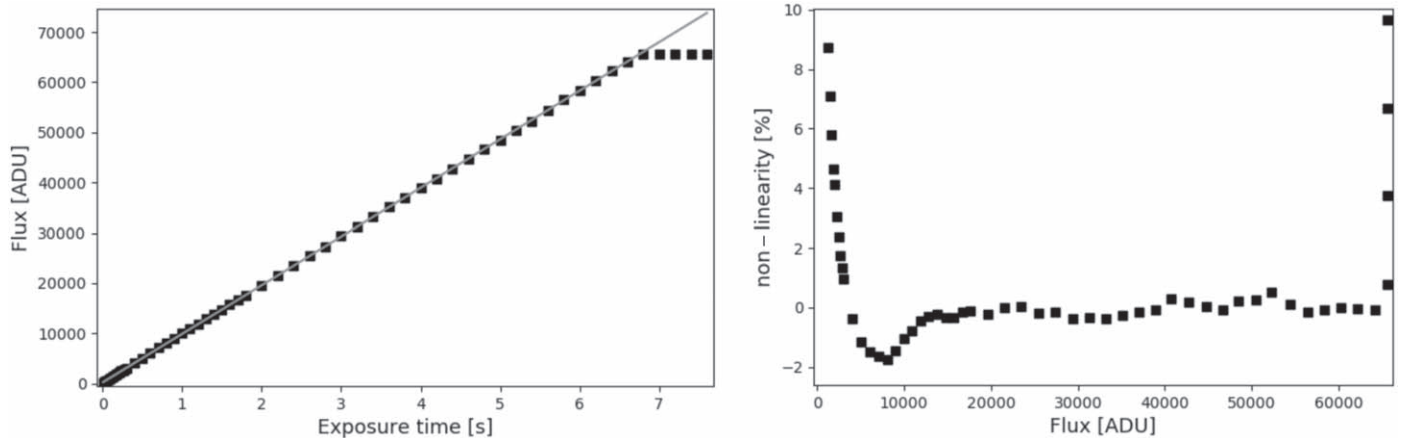


Figure 3. Linearity of the Photometrics PrimeBSI camera shown in the left-hand plot for the full well depth and in the right-hand plot for the flux range between the two amplifiers. The flux was measured in the central 48×48 pixel sized area for different exposure times (black dots). For each exposure time, five flat field images were taken and then normalized and median combined. A linear fit was applied to the data points (gray line). The nonlinearity shows the deviation of the data points to the linear fit, scaled by the flux.

using the emission lines (ThAr), measuring the longitudinal position of the camera when either blue or red lines are in focus. The camera is then tilted accordingly. With the doublet lens, a tilt about 20 degrees is required.

3.5. Data Reduction and Analysis

The spectrograph data reduction system has been written for the flexible reduction of cross-dispersed high-resolution data, such that its order tracing is as flexible as possible, in order to accommodate a variety of different components and setups. For example, the software is designed to cope with a variety of resolutions, order separations, overlaps and curvatures; as well as over/under sampling. It can be used with any type of calibration source once an initial wavelength solution has been found through the identification of some known-wavelength spectral lines. The philosophy has been that once a wavelength solution exists for one configuration a new nearby solution might be found relatively easily given knowledge of the expected known wavelength spectral lines. The data reduction software known as HIFLE⁹ is available on github⁹ and described in Errmann et al. (2020).

3.6. Calibration

For order tracing and flat-fielding we use a stabilized Tungsten lamp (Thor Labs SLS201L/M). Initially we used a so-called “high intensity fiber light source” (Thorlabs OSL1-EC), however, this lamp had rather limited red throughput. The relative system efficiency of the Tungsten lamp along with the camera and fiber throughput can be seen in Figure 4, which illustrates the overlapping spectral orders provided using the flat-field lamp. However, given the strong decline in efficiency toward blue and

red spectral orders this means that multiple flat fields must be taken in order to obtain good quality data in these regions. We found that although the color of the lamp is relatively stable, the intensity of the lamp drops by approximately 10% during the first 30 minutes after switching it on. We also use the Tungsten lamp along with a standard optical power meter (Thor Labs PM100D) to measure the spectrograph throughput from the bifurcated fiber input through the spectrograph to the detector of between 4% and 8% depending on details of components.

For wavelength calibration reference we use a Thorium Argon lamp (P858A—hollow cathode lamp—Thorium with Argon gas fill from Photron). This typically gives around a few thousand potentially usable calibration lines across the optical regime, e.g., the left-hand side of Figure 5 shows lines identified from the reference catalog (in red) used to create the wavelength solution. The remaining lines of the reference catalog, not used for fitting the solution, are shown in green. The right-hand side of Figure 5 shows two images. The left-hand one is from HARPS (showing three orders with dual ThAr feed) and the right-hand one from this spectrograph (showing four orders). For the redder orders ThAr shows a smaller number of very bright lines and a comparison between ThAr and UrNe lines (e.g., Ramsey et al. 2008) indicates a greater line density would be available by using the larger line density available from a UrNe lamp and indeed the output from ThAr and UrNe; might easily be coupled together. However, it is likely that the development of laser combs and perhaps particularly more affordable devices like the Better et al. (2016) photonic comb will be the most appropriate calibration.

3.7. Fiber Input and Modal Noise

We introduce light into the spectrograph by means of one fiber for the target and one for the reference source. This is achieved with two $10 \mu\text{m}$ core 0.1 numerical aperture multimode fibers

⁹ <https://github.com/ronnyerrmann/HIFLE>

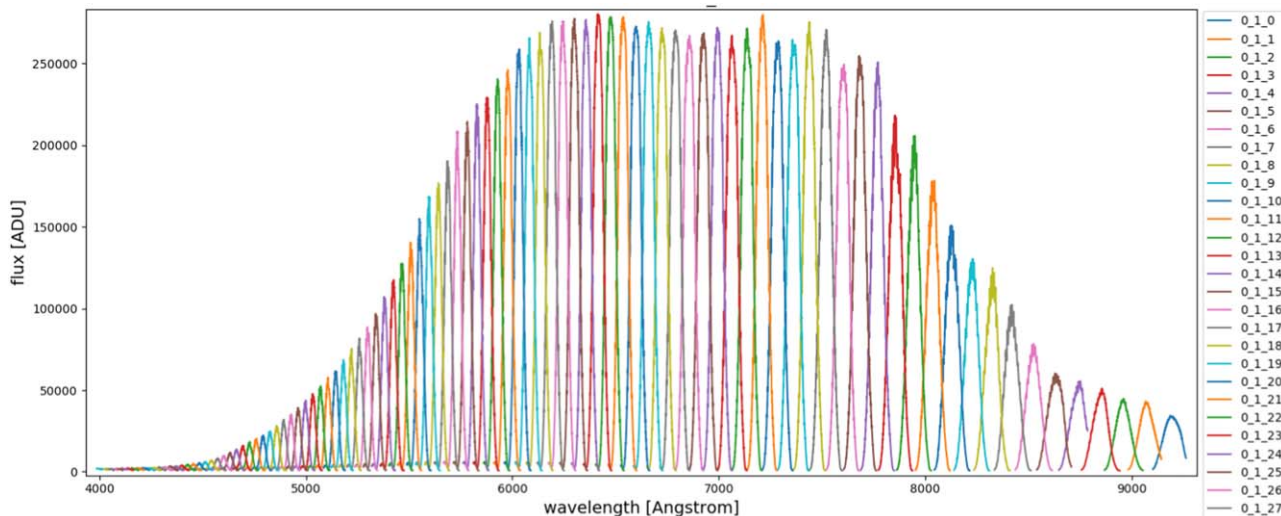


Figure 4. The plot shows overlapping spectral orders producing using a flat-field lamp.

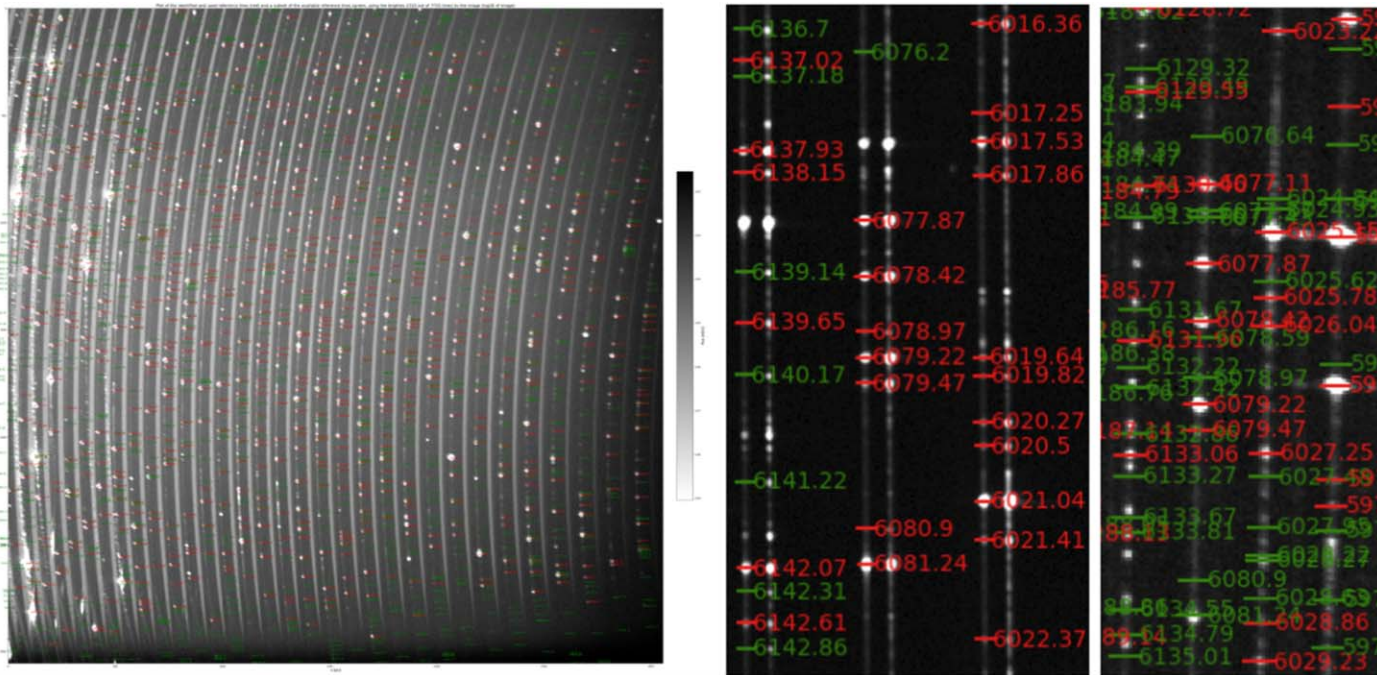


Figure 5. The left-hand image shows an image (log10 gray scale) from our spectrograph showing the continuous orders of a flat-field lamp and simultaneously fed by a ThAr calibration lamp. The right-hand images show an image from HARPS (three orders with simultaneous ThAr in both fibers) on the left and our spectrograph image on the right (four orders with a single fiber input). ThAr lines are automatically identified by the pipeline from the reference catalog (in red) and used to create the wavelength solution. The remaining lines of the reference catalog, not used for fitting the solution are shown in green.

(Thorlabs FG010LDAFBUNDLE) supplied by Thorlabs as a “custom 1×2 fanout bundle” from their range of bifurcated fiber bundles. Each fiber is contained in a protective jacket (Thorlabs FT061PS). These two fibers are combined in a common end connector jacket (also inside FT061PS protective cable) which is connectorised with common end connectors (FC/PC, 30260G3). The reference fiber is connected directly into a ThAr or Tungsten

flat-field lamp. The target fiber is usually connected into a Fiberbench Beamsplitter Module (Thorlabs FBT-50NIR- 50:50) which allows for flexible connection to sky fiber or another calibration source. We find that the fibers used (FG010LDA) have a peak throughput of 75% where we measure the absolute throughput of fibers as part of our fiber characterization experiments (e.g., Choochalem et al. 2021).

We can get light from the Sun into the laboratory by imaging onto a 5 mm ball lens with a 10° field of view (Thorlabs 43–412) connected to a 15 m long $50\ \mu\text{m}$ graded index 0.22 numerical aperture FC/PC cable (Thorlabs M42L15). The large field of view of the ball lens means that tracking errors should not compromise obtaining integrated solar disk light. Unfortunately, we found that the field of view was so large that light scattered by nearby clouds noticeably degraded the quality of our signal and so observations were only attempted when skies were mostly clear. Clouds that do not uniformly cover the Sun during an integration can lead to a significant solar rotation residual since the variation in the velocity across the disk of the Sun is $2\ \text{km s}^{-1}$. Thus, although the Sun is an obvious target for our experiments (e.g., Ramsey et al. 2008) this variation across the disk, along with clouds and a location which is rather prone to wind shake currently leads to an rms between 10 s exposures of $15\ \text{m s}^{-1}$ but can only be maintained for a few minutes. We have achieved slightly better results on the Moon ($14\ \text{m s}^{-1}$ with one minute exposures over 20 minutes). However, instabilities in our guiding and telescope equipment along with a lack of opportunity have so far limited our on-sky data.

We have found that in our instrumental setup, modal noise can be a significant issue. It can be a strong function of wavelength, temperature and even caused by the small agitation induced for example by the laboratory air conditioning fans. In the upper plot of Figure 6 with appropriate scaling and zooming, modal noise can for some wavelengths even be seen in raw data from the camera. The upper plot of Figure 6 presents an illustration of the wavelength dependence of the problem. The issue of modal noise is a well known one for high resolution spectrographs and has been examined in substantial detail; there are a number of potentially mitigations that may be made though no “silver bullet” (e.g., Ishizuka et al. 2016; Blinda et al. 2017; Petersburg et al. 2018). One of the best options would appear to be the appropriate agitation of the fiber in order minimize the effects of modal noise. While we did find this effective our available mechanical solution introduced unwanted vibrations into the setup. Thus instead we deploy an optical solution to the problem by using a mirror galvanometer system.

We use silver coated mirrors (Thorlabs GVS002) and a function generator (Tektronix AFG1022) to apply appropriate patterns of frequencies and amplitude in order to apply a small movement to the beam so that the beam position is changed slightly and thus the illumination of the fiber carrying the light to the spectrograph is altered. We typically use this in 10–100 Hz range with voltages of 20–50 mV. In Figure 7, the top plot shows a schematic of the arrangement used to test the impact of modal noise, the middle plot shows the reality on the optical bench of the different components and the lower plot illustrates the improvement available by modulation of the beam. While this system is effective, we note that in order to optimize the reduction in modal

noise, we need to introduce very significant movement of the beam which then causes a significant loss of throughput. In the case of this plot by a factor of about two in throughput and so this system requires further optimization (C. Boonsri et al. 2020, in preparation) and may not produce as robust results as might be achieved with a double scrambler. Many of our problems are known consequences of using such small fibers. For example they are more difficult to handle and more prone to focal ratio degradation and guiding errors (e.g., Kannappan et al. 2002). They also provide significant differences in potential signal-to-noise as a function of core diameter and geometry (e.g., Sablowski et al. 2016). These issues are closely related to our fiber tapering experiments (Choochalerm et al. 2021).

3.8. Active Stabilization

The beam is turned through 90° toward the camera using a right-angle prism mirror (Thorlabs MRA20-G01). It is mounted on an XY translation stage consisting of a Kinematic Mount (KM200T-SM2), a Kinematic Prism Mount (KM200PM/M) and a Reflecting mirror Mount (KM200CP/M). Its position can be adjusted by piezo inertial actuators (Thorlabs PIK10) which offer movements of 20 nm and “no backlash” in a compact package.

Our active stabilization system uses telescope guiding software (Cyanogen Imaging® MaxIm DL Pro, hereafter MaxIm DL¹⁰) to detect the position of a ThAr line and this “star like” reference image is used as a “guide star.” The ThAr image position on the detector is then used to control XY actuators (Thorlabs) on the turning mirror to stabilize the spectrum of the object on the detector. Figure 8 shows a screen capture of the control computer, the camera control window in the top right indicates, among other things, that the image (an arc line) is being tracked and it displays the camera information along with centroid displacement of the image. The other windows monitor the image. In the top left is the image that is being tracked along with a circular apertures for which statistics are reported in the top middle window. The lower right window indicates the corrections made by the actuator based on the errors of the centroid reported in the camera control window. The bottom left plot shows the centroid behavior in x and y with no tracking and then once tracking has been triggered, a fairly rapid adjustment of the centroid position to the chosen baseline can be seen.

The guiding loop to control the actuators is written in visual basic using the .Net APIs and uses the Visual Studio along with the guiding function of MaxIm DL. This can be used in single or multi-guide star mode. MaxIm DL allows a variety of different guiding functionalities of guiding from automated single- or multi-star to fully defined by the user. MaxIm DL is used in “single-” or “multi-star” autoguiding mode to capture

¹⁰ <https://diffractionlimited.com/product/maxim-dl/>

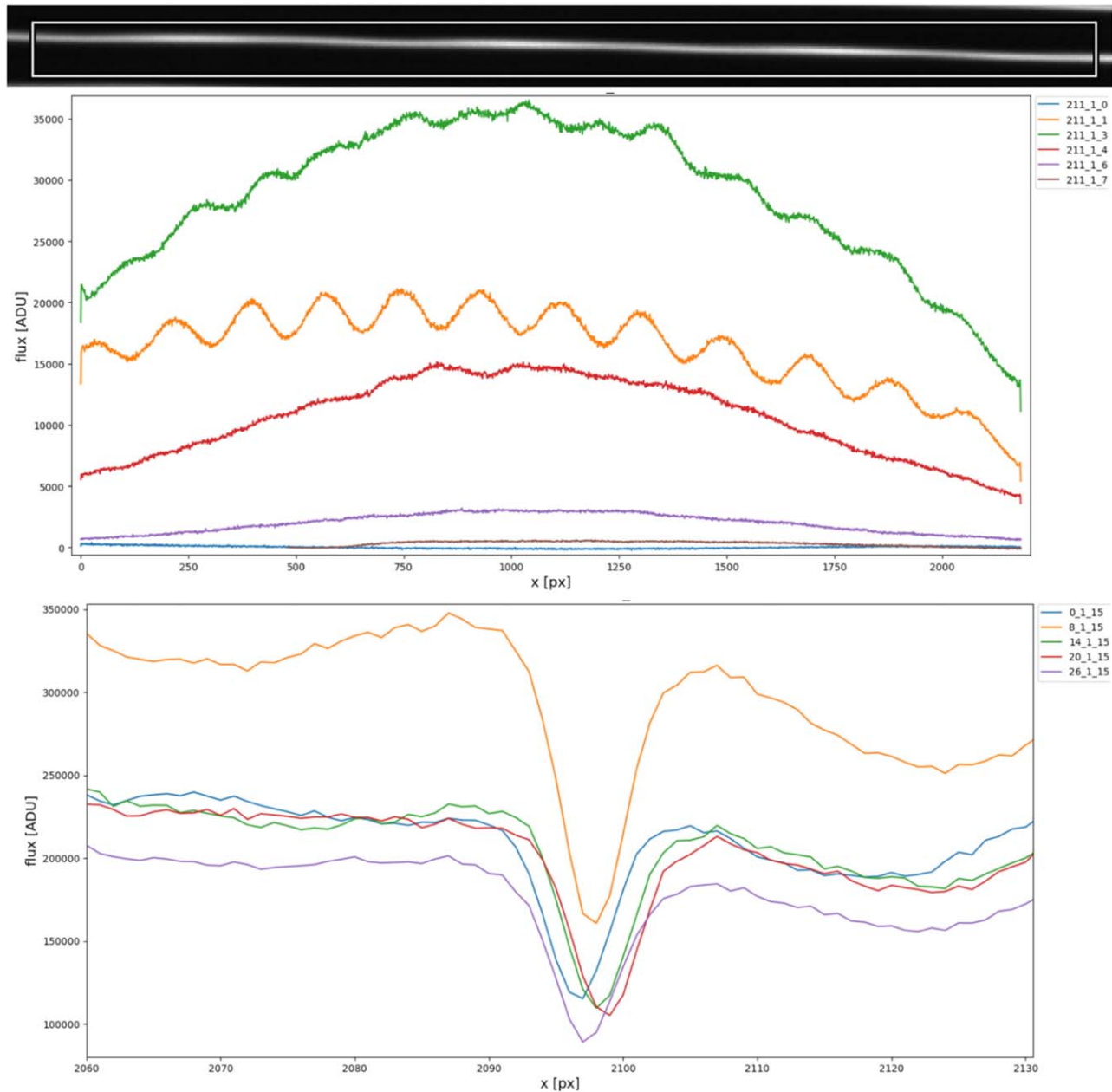


Figure 6. The plots illustrate the impact of modal noise on the spectra. The upper plot shows a zoom in of a raw frame where the trace of spectrum (in white and gray against black background) can be seen as apparently periodic features of substantial strength when the spectra are scaled appropriately. These periodic features can also readily be seen in the extracted spectra. The middle plot shows spectral extractions of different wavelength regions: (blue, 900 nm), 15 (orange, 760 nm), 30 (green, 650 nm), 45 (red, 570 nm), 60 (violet, 510 nm), 75 (brown, 460 nm). The lower plot shows a zoom in on an iron line (FeI at 667.8nm) in the Sun prior to wavelength correction by ThAr where the fiber illumination has been adjusted to maximize the impact of modal noise on a spectral line.

the images and measure the positions of the “guide stars.” The guiding loop to control the actuators is written in C# and is available on Github.¹¹ It uses the Thorlabs Kinesis .Net APIs and uses MaxIm DL’s COM interface to access the guiding errors as the input to a PID control loop. The errors are

dependent on the exposure (signal to noise) so optimization of time constants is required. Our current implementation of the loop uses Kp proportional terms ($x = 10, y = 20$), Kp integral (steady state error) terms ($x = 0.2, y = 0.2$), Kp derivative (dampening) terms ($x = 0.1, y = 0.1$), an iMax limit for integral to prevent wind-up of $x + y = 1$, and a Minimum Move of $x + y = 2$. The control loop code is provided at

¹¹ <https://github.com/bayfordbury-observatory/EXOhSPEC>

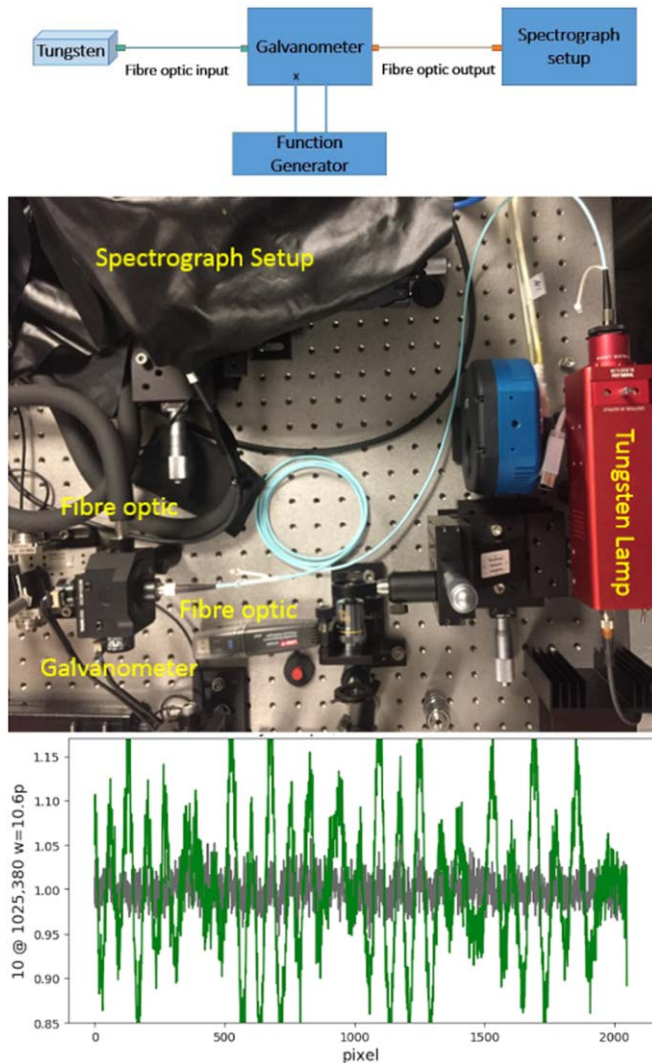


Figure 7. The upper image shows the schematic layout of the spectrograph with galvanometer, the middle image shows the galvanometer on the bench (immediately above the written galvanometer label) and the lower plot gives an example of the impact of modal noise with and without the galvanometer operating.

One of the key facets of a radial velocity spectrograph is long-term temperature, pressure and humidity stability and to this end modern spectrographs typically work in a vacuum and are specified to have mK temperature control. In order to check the stability of the current setup, we split the light from the ThAr lamp into two beams and feed the target and calibration fibers separately with the same lamp. This procedure is similar to the nightly calibration procedure of HARPS.¹² We used continuous 10 s ThAr exposures. Figure 9 shows the measured difference in radial velocity between the target and calibration fibers over 100 minutes. The control loop was switched off

¹² <https://www.eso.org/sci/facilities/lasilla/instruments/harps/inst/calibrations.html>

until 22 minutes, hence creating offsets of several tens of a pixel (beyond the plotted scale). Once switched on the control loop effectively corrects for the changes induced by the regular cycle of the air conditioning system, as measured by the change in humidity. The green points show difference in signal between the two calibration fibers. The rms of the green points over the period is 0.005 pixel. However, with the current setup small variations cannot be corrected due to the response time of the loop and hysteresis of the elements. When the air conditioning system is switched off the rms can be reduced further, however, an rms below 0.0035 pixel (4 m s^{-1}) is not reliably achieved with the current set up. Optically, the axis alignment of the actuators is currently approximately 60 deg from one another, rather than orthogonal. Also the detailed performance of these actuators is not linear at small displacements due to friction and hysteresis. The current step size of the actuators is also rather coarse as one step is approximately 0.005 pixels. Although this and the current control loop settings work relatively well to follow the humidity changes, they can over- and under-correct and the system needs to be redesigned to reach a significantly higher level of sensitivity.

We can compare these results with those found for HARPS calibration. Following a similar analysis using routine calibration data taken from the HARPS archive, we find the same procedure yields an rms scatter of 0.7 milli-pixel (0.6 m s^{-1}). For this experiment, the beam splitter had a rather low throughput in the blue wavelength range and so only lines redder than 510 nm were available for the wavelength solution, which also adds error to the quality of the underlying wavelength solutions which are being compared. For example, looking at the same wavelength range and using the same HiFLEX pipeline (Errmann et al. 2020), the wavelength solution for the EXOhSPEC prototype finds 540 lines to use, whereas for the HARPS data finds 1930 lines to use. The difference in the number of lines can be attributed to a number of factors perhaps particularly the optics (especially the use of doublet lens), quality of the ThAr lamp (Lo Curto 2017) but more simply our short ThAr exposures. For these experiments the sCMOS camera used a firmware version with a maximum of 10 s exposure rather than 40 s used by HARPS. Longer exposures would enable the robust identification of many fainter lines which become available for longer ThAr exposures.

For our current implementation of the prototype we rely on MaxIm DL software which brings some compromises. For example, the range of cameras for which software drivers exist is limited. In the terms of the active stabilization system we have tried the available default guiding options and find improvement in consistency from using “multi-star” (multiple ThAr lines) rather than the other available default options. However, more robust guiding and thus better stability might also be available by optimization of the corrective image shifts given to the actuators by Visual Studio. For example, image

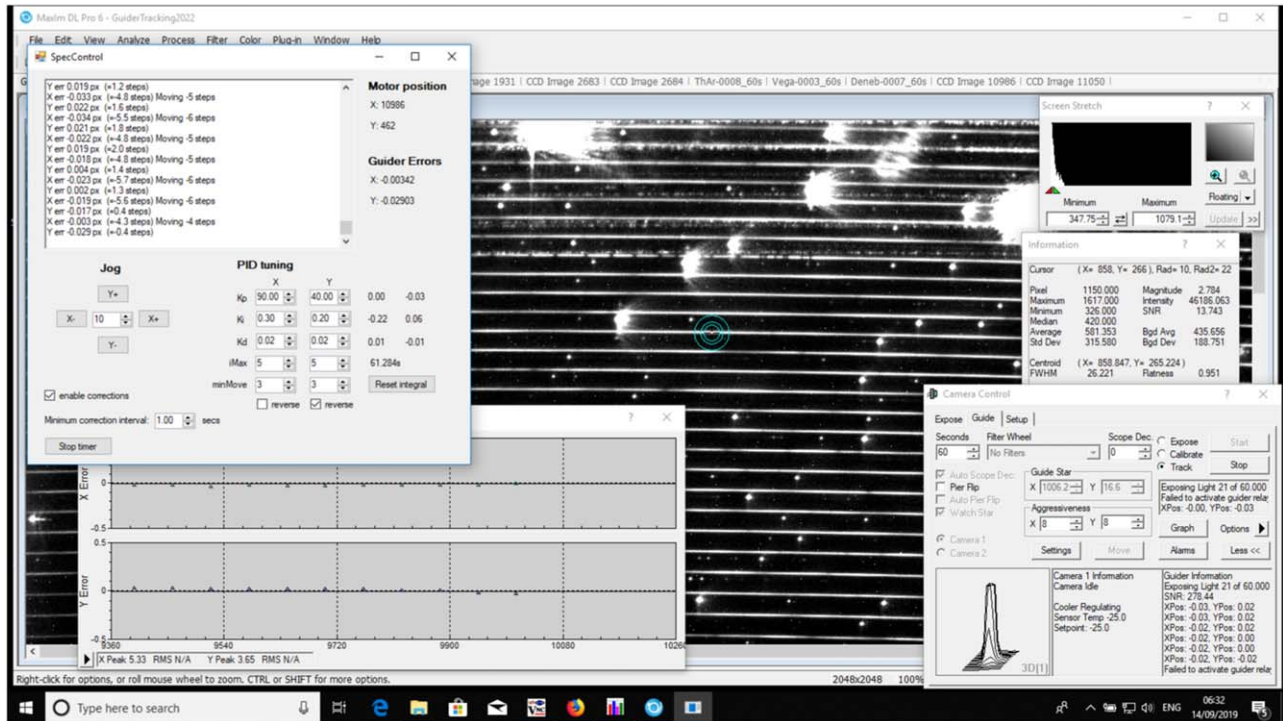


Figure 8. Screen capture of the control computer showing the feedback system in operation. The main frame shows the raw image frame with a flat field lamp (a Thorlabs OSL1-EC with low red throughput enabling arc lines to be easily seen) and ThAr both in the target fiber. The camera control window in the top right indicates among other things that the image (an arc line) is being tracked (as a guide star) and indicates the camera information along with centroid displacement of the image. The lower left window indicates the corrections made by the piezo actuators based on the deviations of the centroid reported in the camera control window. The bottom right plot shows two separate plots of the displacement of the arcline in x and y with time. Once tracking has been switched on a fairly rapid adjustment of the centroid position occurs to bring it to (0,0).

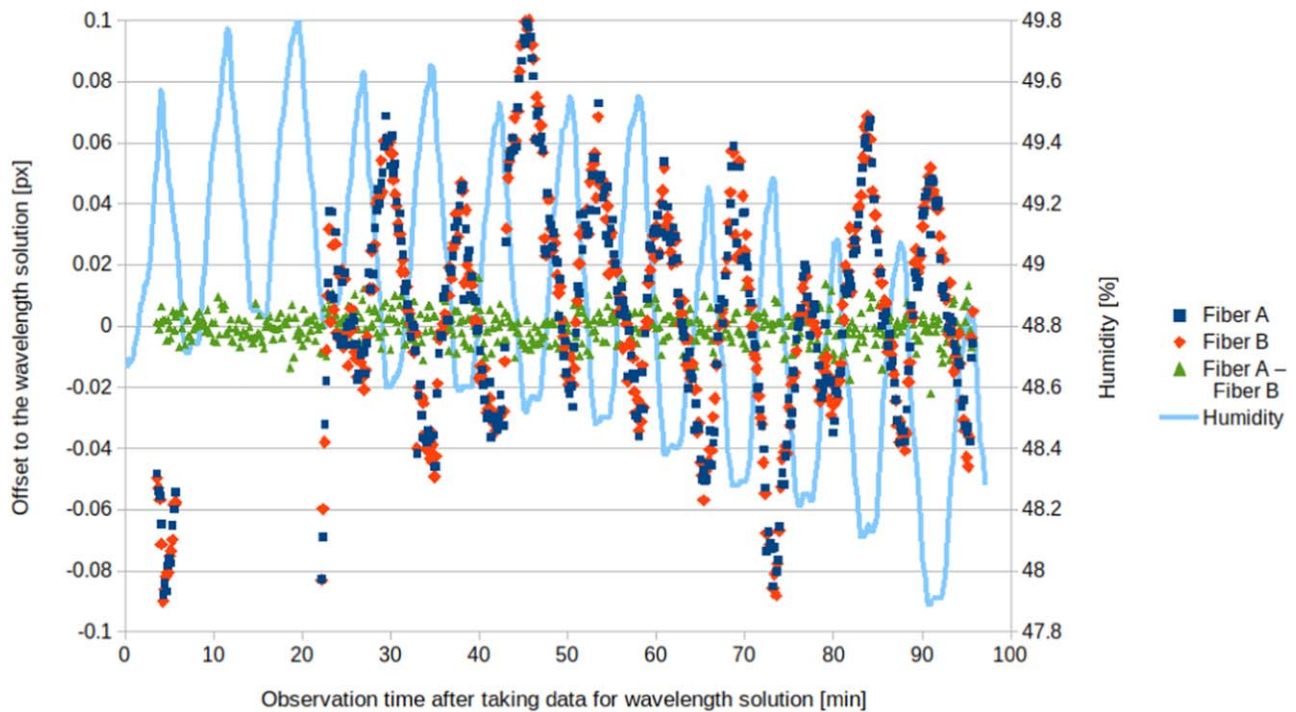


Figure 9. Offsets to the wavelength solution caused by humidity changes in the spectrograph arising from the laboratory air conditioning system over a timescale of 100 minutes when both fibers are fed by the same calibration lamp.


processing outside of MaxIm DL might follow a methodology like (Gunther et al. 2017) and limit the lines used for centroiding to an optimized set of ThAr lines (e.g., based on Lovis & Pepe 2007).

4. Conclusion

The process of building a small stable high resolution spectrograph using commercially available components has involved moving from (1) a variety of SLR camera lenses to an achromatic doublet, (2) standard input fiber, to a bifurcated fiber, (3) iteration of prisms for improved anti-reflection coating and appropriate cross-dispersion properties, (4) a replica grating from Thorlabs to larger more efficient Richardson one, (5) control of modal noise through introduction of a galvanometer, (6) use of a CMOS rather than a CCD camera and (7) inactive to active control with second order correction. We have explored a number of system options and demonstrate how a relatively small and inexpensive spectrograph built from off-the-shelf components can achieve high resolution and reasonable optical quality as judged relative to the HARPS spectrograph. A key finding is that precisions below 5m s^{-1} can be achieved by using commercial autoguiding software to determine the appropriate feedback to maintain stability. Further work is required to demonstrate robust system performance in an astronomical setting on a telescope.

We are grateful for support of this project through Newton fund grants from STFC (ST/P005667/1 and ST/R006598/1), to John Collins for his donation of his Celestron Edge HD, to Peter Beck for his donation of the Tungsten lamp to the project and to Christophe Buisset and Suparek Aukkaravittayapun for supporting this project at NARIT. G.A.E. acknowledges a Ramón y Cajal Research fellowship. We are glad to acknowledge the use of calibration data obtained from the ESO Science Archive Facility from proposal 072.C-0488(E) based on nights 2004-07-10 to 2004-07-31. The original version of this manuscript was significantly improved by the insights of the anonymous referee.

ORCID iDs

H. R. A. Jones  <https://orcid.org/0000-0003-0433-3665>
 G. Anglada-Escudé  <https://orcid.org/0000-0002-3645-5977>
 R. Ermann  <https://orcid.org/0000-0002-3683-1952>

References

- Baker, C., Anglada-Escude, G., Jones, H., & Martin, W. 2019, *Proc. SPIE*, 11117, 111171
- Becker, J. M. 1976, *Natur*, 260, 227
- Bettters, C. H., Hermouet, M., Blanc, T., et al. 2016, *Proc. SPIE*, 9912, 99126
- Blinda, N., Conoda, U., & Wildi, F. 2017, arXiv:1711.00835
- Bond, C., Brown, D., Freise, A., & Strain, K. A. 2016, *LRR*, 19, 3
- Buikema, A., Cahillane, C., Mansell, G. L., et al. 2020, arXiv:2008.01301
- Butler, R. P., Jones, H. R. A., Feng, F., et al. 2019, *AJ*, 158, 6
- Butler, R. P., Marcy, G. W., Williams, E., et al. 1996, *PASP*, 108, 500
- Calderone, G., Baldini, V., Cirami, R., et al. 2016, *Proc. SPIE*, 9913, 99132
- Campbell, B., & Walker, G. A. H. 1979, *PASP*, 91, 540
- Campbell, B., Walker, G. A. H., & Yang, S. 1988, *ApJ*, 331, 902
- Choochaleern, P., et al. 2021, OptFT, submitted
- Cosentino, R., Lovis, C., Pepe, F., et al. 2012, *Proc. SPIE*, 8446, 84461V
- Crane, J. D., Shectman, S. A., & Butler, R. P. 2006, *Proc. SPIE*, 6269, 626931
- Errmann, R., Cook, N., Anglada-Escude, G., et al. 2020, *PASP*, 132, 064504
- ESA 2014, JUICE Study Definition Report, ESA/SRE(2014), 1, <https://sci.esa.int/web/juice/-/54994-juice-definition-study-report>
- Feng, F., Lisogorskyi, M., Jones, H. R. A., et al. 2019, *ApJS*, 244, 39
- Gunther, M., Queloz, D., Gillen, E., et al. 2017, *MNRAS*, 472, 295
- Haynes, D., Haynes, R., Olaya, J. C., & Laval, S. 2012, *Proc. SPIE*, 8450, 84503
- Ishizuka, M., Kotani, T., Nishikawa, J., et al. 2016, *Proc. SPIE*, 9912, 99121Q
- Kannappan, S. J., Fabricant, D. G., & Hughes, C. B. 2002, *PASP*, 114, 795
- Kawinkij, A., Prasit, A., Buisset, C., et al. 2019, *Proc. SPIE*, 11116, 111161G
- Koch, A., & Woehl, H. 1984, *A&A*, 134, 134
- Latham, D. W., Mazeh, T., Stefanik, R. P., Mayor, M., & Burki, G. 1989, *Natur*, 339, 38
- Lhospice, E., Buisset, C., Jones, H. R. A., et al. 2019, *Proc. SPIE*, 11117, 111170Z
- Lizon, J. L., Iwert, O., Deiries, S., et al. 2016, *Proc. SPIE*, 9908, 990866
- Lo Curto, G. 2017, Instrument Talk: HARPS, Zenodo, doi:10.5281/zenodo.887265
- Lovis, C., & Pepe, F. 2007, *A&A*, 468, 1115
- Lovis, C., Snellin, I., Mouillet, D., et al. 2017, *A&A*, 599, 16
- Pepe, F. 2018, *Proc. SPIE*, 10702, 107020X
- Pepe, F., Cristiani, S., Rebolo, R., et al. 2020, arXiv:2010.00316
- Pepe, F., Mayor, M., Delabre, B., et al. 2000, *Proc. SPIE*, 4008, 582
- Peters, A., Chung, K. Y., & Chu, S. 2001, *Metro*, 38, 25
- Petersburg, R. R., McCracken, T. M., Eggermann, D., et al. 2018, *ApJ*, 853, 181
- Radovan, M. V., Cabak, G. F., Laiterman, L. H., Lockwood, C. T., & Vogt, S. S. 2010, *Proc. SPIE*, 7735, 77354K
- Ramsey, L. W., Barnes, J., & Redman, S. L. 2008, *PASP*, 120, 887
- Sablowski, D. P., Pluschke, D., Weber, M., Strassmeier, K. G., & Jarvinen, A. 2016, *AN*, 337, 216
- Schroeder, D. J. 1967, *ApOpt*, 6, 11
- Schroeder, D. J. 1970, *PASP*, 82, 1253
- Schroeder, D. J. 1987, *Astronomical Optics* (San Diego: Academic)
- Schroeder, D. J., & Anderson, C. M. 1971, *PASP*, 83, 43
- Seifahrt, A., Stürmer, J., Bean, J. L., & Schwab, C. 2018, *Proc. SPIE*, 10702, 107026
- Struve, O. 1952, *Obs*, 72, 199
- Tull, R. G. 1998, *Proc. SPIE*, 3355, 387
- Vogt, S. S., Allen, S. L., Bigelow, B. C., et al. 1994, *Proc. SPIE*, 2198, 362
- Wolszczan, A., & Frail, D. A. 1992, *Natur*, 355, 145
- Zhan, H., Zhang, X., & Cao, L. 2017, *JINST*, 12, C04010